ISSN 0023-1584, Kinetics and Catalysis, 2006, Vol. 47, No. 4, pp. 624–637. © MAIK "Nauka/Interperiodica" (Russia), 2006.
Original Russian Text © I.Yu. Shchapin, V.V. Vasil'eva, A.I. Nekhaev, E.I. Bagrii, 2006, published in Kinetika i Kataliz, 2006, Vol. 47, No. 4, pp. 642–656.

SECOND INTERNATIONAL CONFERENCE ON HIGHLY ORGANIZED CATALYTIC SYSTEMS (MOSCOW, JUNE 14–17, 2004)

On a Possible Radical-Cation Mechanism of the Biomimetic Oxidation of the Saturated Hydrocarbon 1,3-Dimethyladamantane in a Gif-Type System Containing a Fe^{2+} Salt, Picolinic Acid, and Pyridine

I. Yu. Shchapin[a,b], V. V. Vasil'eva[c], A. I. Nekhaev[c], and E. I. Bagrii[c]

[a] *Faculty of Chemistry, Moscow State University, Moscow, 119899 Russia*
[b] *Karpov Research Institute of Physical Chemistry, Moscow, 103064 Russia*
[c] *Topchiev Institute of Petrochemical Synthesis, Russian Academy of Sciences, Moscow, 117912 Russia*

Received September 30, 2004

Abstract—Based on an analysis of the ratio between the final products of the oxidation of 1,3-dimethyladamantane (1,3-DMA) with hydrogen peroxide under new catalytic conditions, an EPR-spectroscopic study of the 1,3-DMA radical cation under model radiation-chemical conditions, and the results of PM3 quantum-chemical calculations, a new mechanism was proposed for the biomimetic oxidation of the saturated hydrocarbon. This mechanism involves the intermediate formation of the 1,3-DMA radical cation, in which a tertiary C–H bond is selectively activated. Next, oxene (oxygen atom) is inserted into this C–H bond to form a tertiary alcohol. It was found that a comparison of the composition of final products in the oxidation of saturated hydrocarbons under conditions of a real chemical experiment with the structure and reactivity of their radical cations under model radiation-chemical conditions can be a methodologically new general technique for the analysis and prediction of the reactivity of saturated hydrocarbons under oxidative conditions.

DOI: 10.1134/S0023158406040197

INTRODUCTION

Hill [1] generally systematized and discussed the possible reaction paths of C–H bond monooxygenation by the metal oxo compounds $L_nM^{(n+2)+}=O$, where M = Cr, Mn, Fe, etc. Figure 1 shows the three main possible reaction paths according to Hill made specific for Fe^{2+} and Fe^{3+} complexes (n = 2, 3) and supplemented (dashed lines) with the yields of reactive species (neutral radical (1c) and radical cation (2b)) into the bulk of the chemical system, as well as the deprotonation reaction of radical cation (2a) and the single-step concerted insertion of the oxygen atom into the C–H bond (2c).

The first reaction path is the homolytic cleavage of a C–H bond with the formation of a neutral carbon-centered radical and the OH group coordinated to the iron ion. Next, three possible reaction paths can lead to alcohol formation: the direct abstraction of the OH group from the iron ion by the carbon-centered radical (path 1a), with the intermediate formation of an organometallic compound (path 1b), and with the escape of the carbon-centered radical into the bulk of the chemical system and intermediate hydroperoxide formation (path 1c).

The second reaction path, which occupies a central place in our scheme, as well as in the scheme of Hill, corresponds to a one-electron transfer from the hydrocarbon to a metal complex to form hydrocarbon radical cations. However, in 1989, Hill practically did not consider this reaction path because, in his opinion, there were no reliable examples of the thermal or chemical oxidation of unbranched alkanes in solutions by an electron-transfer mechanism; correspondingly, there was no data for comparison [1]. This situation occurred until more recent times [2].

The third reaction path is the concerted single-step insertion of the oxygen atom into a C–H bond of the molecule. The symbol ≠ in Fig. 1 denotes that the transition-state structure of this process is shown in square brackets. As applied to the monooxygenation of saturated hydrocarbons with the participation of iron-containing monooxygenases, two reaction paths 1b and 3 have been usually compared [1–3]. In both cases, it was predicted that the strength of the C–H bond and the spatial accessibility of this bond to the catalytic center are responsible for the selectivity of enzymatic processes.

The biological oxidation (with the use of bacteria) of adamantane hydrocarbons occurs with 100% selectivity at tertiary C–H bonds with alcohol formation [4]. In contrast to this, the Gif-type oxidation of the above hydrocarbons occurs with 100% selectivity at secondary C–H bonds with ketone formation [1, 5, 6]. An

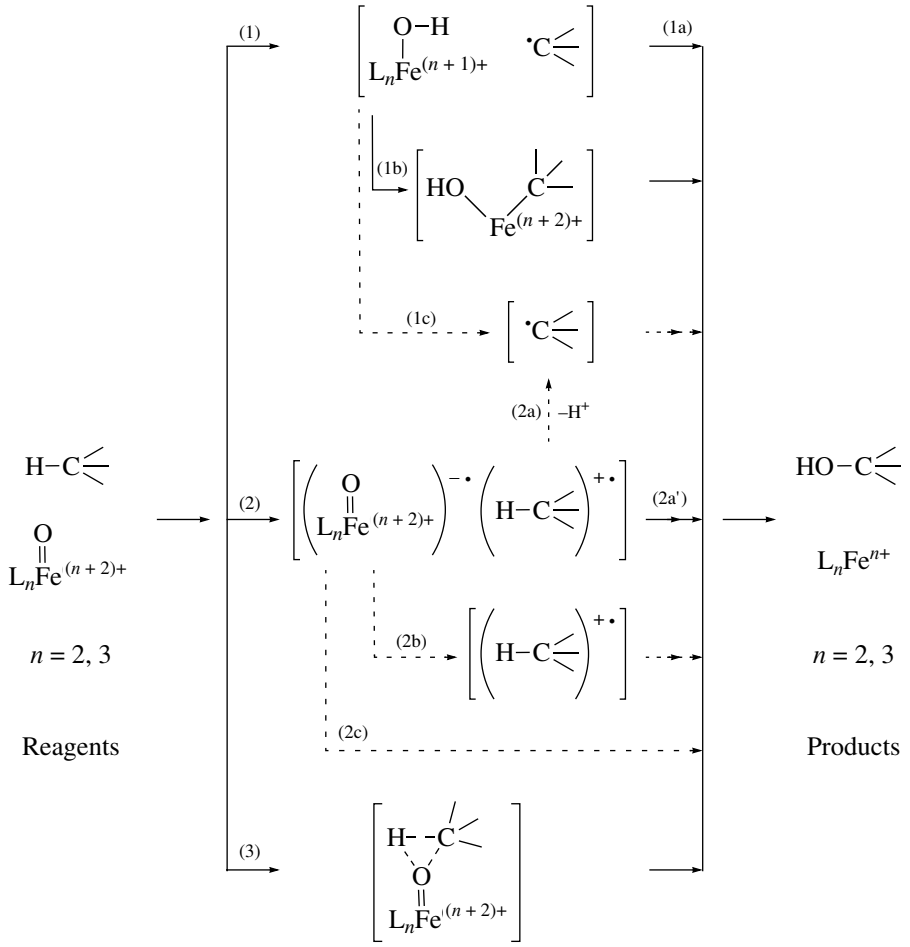

Fig. 1. General reaction scheme of the main possible paths of monooxygenation of C–H bonds in saturated hydrocarbons RH by ferroxo-containing catalytic centers. Dashed lines show our supplements to the systematization of Hill [1] (see the text for details).

intermediate case occurred in the radical oxidation of adamantane: the tertiary and secondary C–H bonds were simultaneously oxidized with approximately equal efficiencies [1, 7, 8]. More precisely, the concentration of the product of adamantane oxidation at tertiary C–H bonds (a tertiary alcohol) normalized to one C–H bond was somewhat greater than the total concentration of a secondary alcohol and a ketone. This was because the strength of a tertiary C–H bond toward homolytic cleavage is lower than that of a secondary C–H bond.

In a Gif-type catalytic system, whose components were an Fe^{2+} salt, picolinic acid (pyridine-2-carboxylic acid), and pyridine, as well as an aqueous acetonitrile solvent and hydrogen peroxide as an oxidizing agent, we found new selectivity of the oxidation of 1,3-dimethyladamantane (1,3-DMA), which is unusual for systems of this type [9]. In place of Gif-type oxidation or radical oxidation, tertiary C–H bonds were oxidized; that is, from the standpoint of positional selectivity, the biomimetic oxidation of a saturated hydrocarbon was performed for the first time. This type of oxidation is inconsistent with either of the two mechanisms proposed previously for Gif-type systems: nonradical (Barton) [1, 3, 5, 6] and radical mechanisms (Stavropoulos) [7, 8]. Thus, we faced the problem of searching and formulating the main signs and concepts of a new mechanism for the selective oxidation of 1,3-DMA in order to explain the selective formation of a tertiary alcohol.

A new area in the selective functionalization of structurally different saturated hydrocarbons related to the generation of their radical cations is currently under intense development [2, 10–12]. In the chemical or electrochemical generation of the adamantane radical cation, a tertiary C–H bond is selectively activated and involved in the subsequent chemical reactions. In particular, it can undergo deprotonation with the formation of a tertiary adamantyl radical [10–16].

The activation selectivity of the tertiary C–H bond of the adamantane radical cation is fully consistent with the selectivity of biological and biomimetic adamantane oxidation at the above C–H bond. This analogy allowed us to hypothesize that a mechanism with the

intermediate formation of radical cations is worthy of consideration because it may be responsible for the high selectivity of biological and biomimetic oxidation of saturated hydrocarbons, including 1,3-DMA, under the new catalytic conditions.

The radical cations of saturated hydrocarbons exhibit high reactivity and undergo rapid chemical reactions in liquid media. At the same time, the radical cations of many organic substrates, in particular, saturated hydrocarbons from all classes, were found stable under model radiation-chemical conditions, where the radical cations were generated in the chemically inert matrices of fluorine- and chlorine-containing Freons and perfluoroalkanes frozen at low temperatures with the use of X-rays or ^{60}Co γ-radiation. This technique provided an opportunity to study the structure and chemical transformations of radical cations using EPR and UV spectroscopy in combination with quantum-chemical calculation data [17].

Note that the reactions of radical cations occurred with 100% selectivity under model radiation-chemical conditions. In many cases, the substrate radical cation underwent deprotonation with the formation of a neutral radical. A fundamentally new fact is that the selectivity of this process depends on the composition of the singly occupied molecular orbital (SOMO) of the radical cation, which is responsible for the unpaired electron density distribution.

The following empirical rule was found: the selective deprotonation of a radical cation occurs by the rupture of the C–H bond that is characterized by the greatest isotropic hyperfine-interaction constant with hydrogen atoms (a_{iso}^{H} > 30–50 G; 1 G = 0.1 mT; spin delocalization effect), as determined by EPR spectroscopy [18–20].

There is a correlation, which explains the reason for this selectivity [20], between the constant a_{iso}^{H} and the elongation (consequently, weakening) of the C–H bond upon the ionization of the molecule (ΔCH = CH_{RC} – CH_{mol}) calculated by ab initio quantum-chemical methods. The greater the constant $a_{iso}^{H} > 0$, the more elongated and weakened the C–H bond of the radical cation and the more reactive this bond.

Thus, in combination with the above correlation, the empirical rule determined for the deprotonation of substrate radical cations under model radiation-chemical conditions allows us to predict the reactivity of radical cations based on both EPR data and the results of quantum-chemical calculations.

The aims of this work were the following: First, to determine the structure and reactivity of the 1,3-DMA radical cation under model radiation-chemical conditions using EPR spectroscopy and quantum chemistry because relevant information for adamantane hydrocarbons is unavailable. Second, to formulate and demonstrate a general procedure for the use of these data for predicting the selectivity of processes with the participation of the radical cations of saturated hydrocarbons under conditions of a real chemical experiment. Third, to apply this procedure to the catalytic system of interest for testing the hypothesis on the intermediate formation of the 1,3-DMA radical cation.

EXPERIMENTAL

A standard procedure was used for studying the 1,3-DMA radical cation in a matrix of Freon 113 ($CFCl_2CF_2Cl$) [17–22]. A solution of 1,3-DMA in Freon 113 with a required concentration (1 vol %) was placed in an EPR ampule of Luch glass (which does not give EPR signals under exposure to ionizing radiation). The ampule was evacuated to a pressure of 10^{-3} Torr by a triple cycle of freezing at 77 K and thawing at room temperature. Next, the ampule was sealed and irradiated with X-rays (40 keV) to a dose of 0.5 Mrad at 77 K. The EPR spectra were measured at 77 K on a modernized RE-1301 spectrometer (Russia). The theoretical simulation of the EPR spectra was performed using the WINSIM software.

The PM3 quantum-chemical calculations were performed using the MOPAC 7.00 program package [23]. The isotropic hyperfine-interaction constants with hydrogen atoms $a_{iso}^{H} = a(H)$ were calculated from Eqs. (1) and (2). The proportionality coefficients $K(H_\alpha)$ and $K(H_\beta)$ were initially found empirically [19] for the MNDO-UNF method and then theoretically substantiated [19, 24] for all NDO-UHF versions. The practical applicability of the coefficients $K(H_\alpha)$ and $K(H_\beta)$ to the PM3 method was demonstrated previously [22].

$$a(H_\alpha) = K(H_\alpha)\rho(H_\alpha), \quad K(H_\alpha) = 415\ \text{G}, \quad \rho(H_\alpha) < 0, \tag{1}$$

$$a(H_\beta) = K(H_\beta)\rho(H_\beta), \quad K(H_\beta) = 850\ \text{G}, \quad \rho(H_\beta) > 0. \tag{2}$$

RESULTS

Figure 2a shows the EPR spectrum of an X-ray-irradiated (at 77 K) 1 vol % solution of 1,3-DMA in Freon 113 ($CFCl_2CF_2Cl$) measured at 77 K. The main characteristic of the spectrum is the occurrence of a doublet with a poorly resolved additional substructure. The difference between the doublet lines is greater than 100 G. The central portion of the spectrum also exhibits a multiplet with a small constant (~8 G) and an unresolved signal from matrix radicals (MRs), which is shown with a dotted line in Fig. 2a. The poorly resolved doublet structure with a splitting of more than 100 G was represented using a model spectrum (Fig. 2b), which corresponds to the 1,3-DMA radical cation: a_{iso}^{H} = 145 (1 H), 40 (1 H), and 20 G (2 H). Figure 2 also shows the

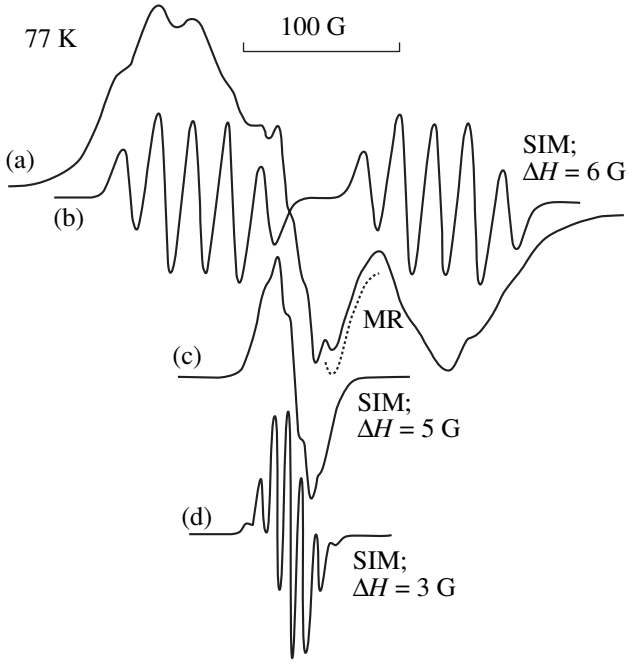

Fig. 2. (a) EPR spectrum of a solution of 1,3-DMA (1 vol %) in Freon 113, which was irradiated with X-rays (0.5 Mrad) at 77 K, measured at 77 K. (b–d) Model (SIM) spectra (the Lorentzian fraction is equal to 20%; ΔH is the line width). The dotted line shows the singlet line of matrix radicals (MR).

(c) poorly resolved and (d) well-resolved model spectra of a multiplet with the constant $a_{iso}^{H} = 8$ G (6 H), which correspond to a tertiary neutral radical of the adamantyl type [22, 25, 26]. Thus, the selective deprotonation of the 1,3-DMA radical cation partially occurs in Freon 113 even at 77 K with the formation of a tertiary neutral radical of the adamantyl type. This observation in combination with the empirical rule allowed us to make the tentative assignment of the EPR spectrum in Fig. 2a to the structure of the 1,3-DMA radical cation with a selected tertiary C–H bond, which is shown in Fig. 3 to participate in the selective deprotonation of the 1,3-DMA radical cation.

In order to provide support for the tentative assignment of the EPR spectrum of the 1,3-DMA radical cation, we performed a complete analysis of the electronic structure of the parent 1,3-DMA molecule and three possible electronic states of the 1,3-DMA radical cation taking into account a decrease in symmetry from C_{2v} to C_s using PM3 semiempirical quantum-chemical calculations. Figures 4 and 5 and Tables 1 and 2 summarize the results.

Figure 4 shows the numbering of 1,3-DMA atoms, which was used for the formation of data in Tables 1 and 2, and the shapes and relative energy arrangements of three upper occupied molecular orbitals, which are orthogonally oriented to each other along the *x*, *y*, and *z* axes. The highest occupied molecular orbital is referred to as HOMO. The above three orbitals (HOMO, HOMO-1, and HOMO-2) are arranged in a narrow energy range (0.34 eV; 1 eV = 23.061 kcal/mol). Each of them can become a singly occupied molecular orbital (SOMO) of the radical cation and form a stable geometric structure in three different electronic states of the radical cation. The next occupied molecular orbital (OMO) of 1,3-DMA in terms of energy has a symmetry of $8B_2$ (HOMO-3) and a much lower energy (−11.69 eV), which is 0.57 eV lower than the energy (−11.12 eV) of the foregoing orbital (symmetry $9B_2$; HOMO-2). Because the ionization of molecules in a condensed medium occurs from high OMOs, we do not consider deeper OMOs starting with the $8B_2$ orbital.

Of the three high OMOs, the following two orbitals are of interest for the assignment of the EPR spectrum of the 1,3-DMA radical cation: HOMO with symmetry $8B_1$ and energy of –10.78 eV and HOMO-2 with symmetry $9B_2$ and energy of –11.2 eV. This is due to the fact that they provide an opportunity for a necessary set of hydrogen atoms (1H · 1H · 2H) to be formed. In the HOMO-1 orbital, the contributions of the hydrogen atoms of the adamantane skeleton (C_{tert}–H) and methyl groups (H atoms in the plane of carbon atoms of an *n*-pentane fragment) of interest are small. They cannot provide a strong elongation and weakening of corresponding C–H bonds upon the adiabatic ionization of the molecule; consequently, they cannot reproduce a

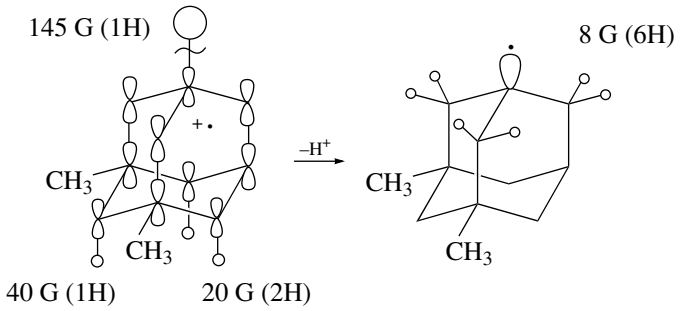

Fig. 3. Selective deprotonation of the 1,3-DMA radical cation under model radiation-chemical conditions.

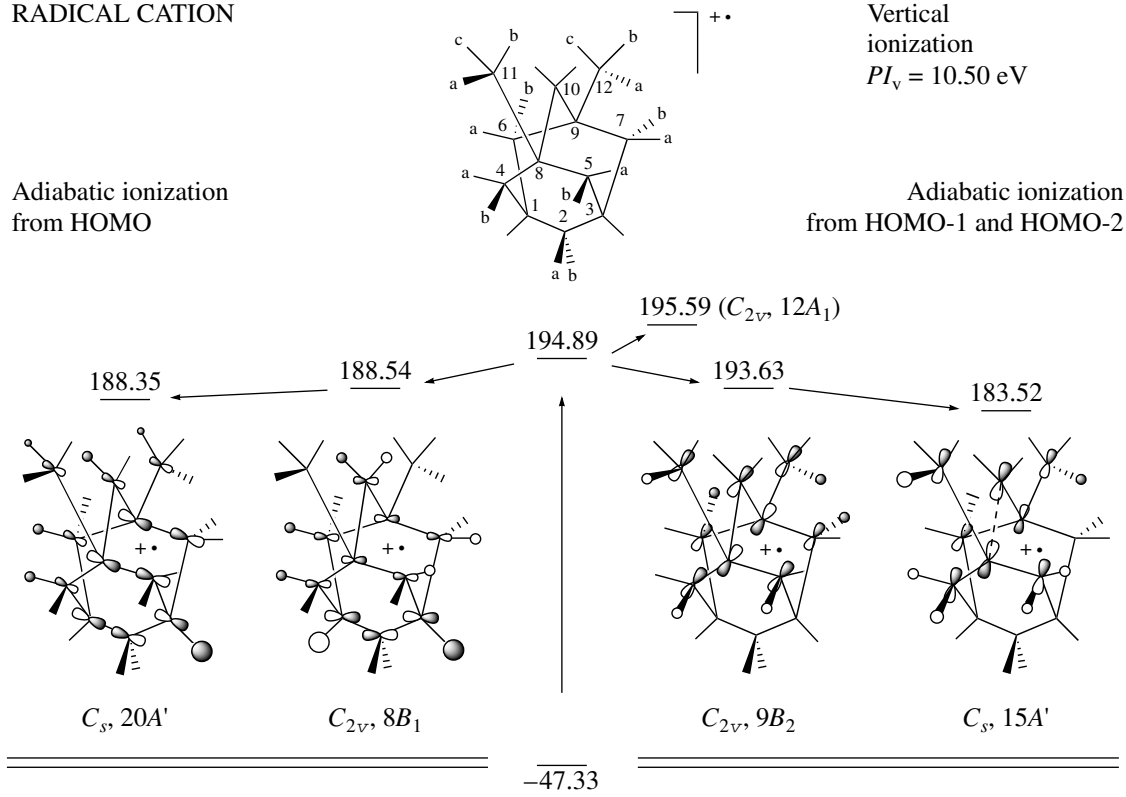

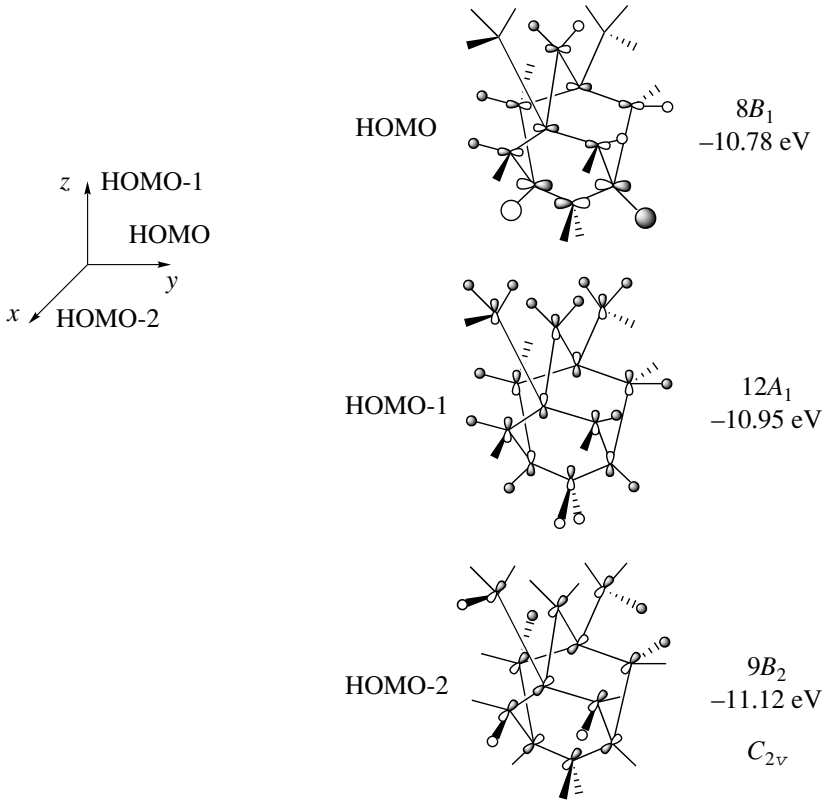

Fig. 4. Schematic diagram for the quantum-chemical calculations of the vertical and adiabatic ionization of the 1,3-DMA molecule.

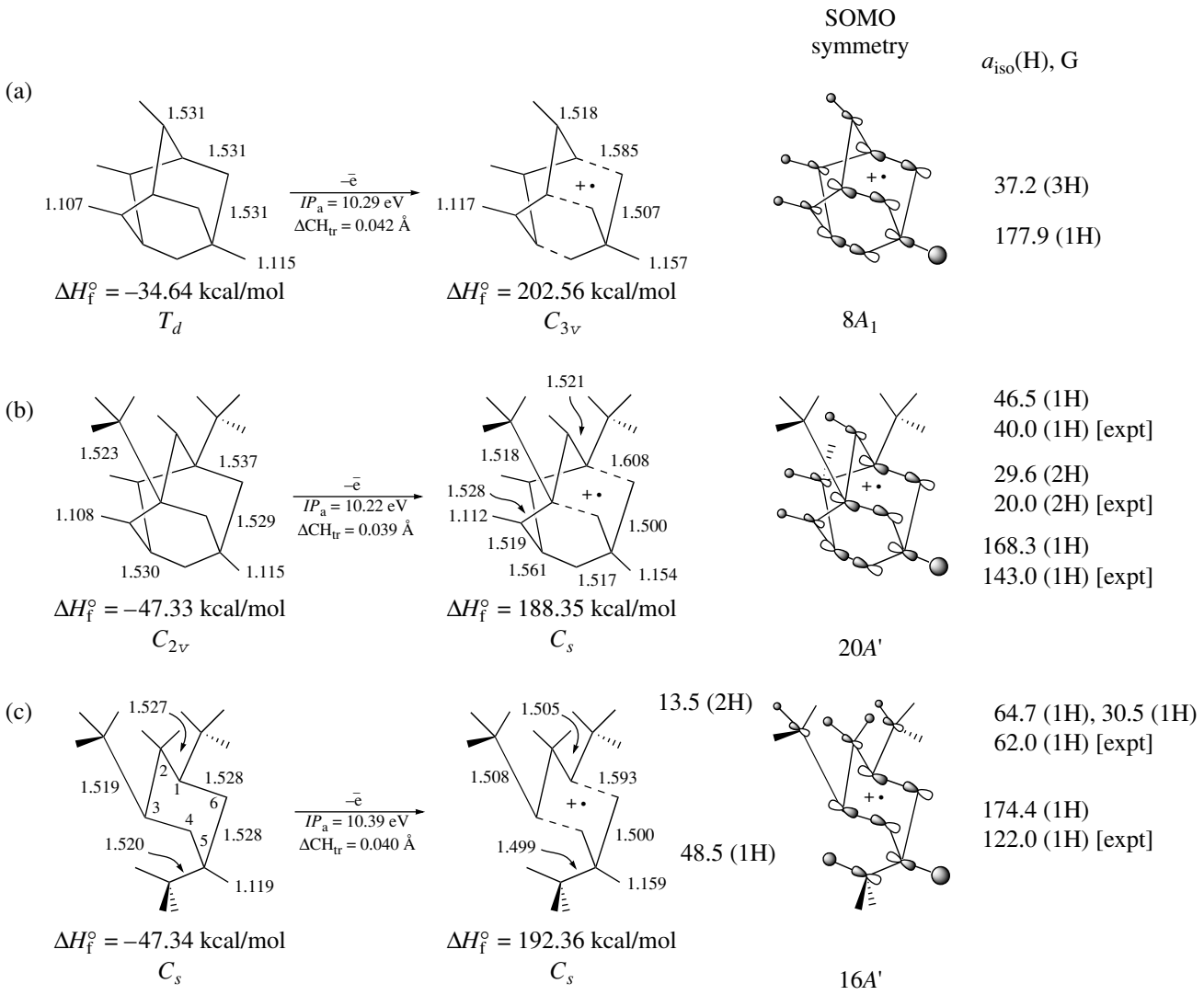

Fig. 5. Parameters of the molecules and radical cations of related structures calculated by the PM3 method: (a) adamantane, (b) 1,3-DMA, and (c) 1,*cis*-3,*trans*-5-trimethylcyclohexane.

great (greater than 100 G) a_{iso}^{H} constant. The HOMO-1 orbital was also excluded from the subsequent procedures of searching for the electronic states of the radical cation with a specified SOMO symmetry. However, for completeness, Fig. 4 and Tables 1 and 2 also give necessary data related to the 1,3-DMA radical cation with a SOMO of symmetry $12A_1(C_{2v})$, which corresponds to HOMO-1.

The vertical ionization potential (PI_v) of 1,3-DMA is 10.50 eV, and the corresponding energy of formation (ΔH_f°) of the radical cation is 194.89 kcal/mol. The calculated value of PI_v is much higher than the experimental value of 9.15 eV (photoelectron spectroscopy) [14]. We did not introduce correction factors for determining the value of PI_v for 1,3-DMA more exactly because this was beyond the scope of this study. In our analysis, the arrangement of various electronic states of the 1,3-DMA radical cation with respect to each other in terms of the energies of formation was important.

The adiabatic ionization of 1,3-DMA from HOMO (Fig. 4, left-hand side) results in the formation of the radical cation with SOMO of the same symmetry $8B_1$ and the energy of formation of 188.54 kcal/mol. As compared with vertical ionization, the energy gain is 6.35 kcal/mol. A decrease in the radical cation symmetry from C_{2v} to C_s results in the structure of interest with SOMO of symmetry 20*A*' and is accompanied by a very small energy gain of 0.19 kcal/mol. On the contrary, with the retention of the initial symmetry C_{2v}, the adiabatic ionization of 1,3-DMA from HOMO-2 (Fig. 4) results in the radical cation with SOMO $9B_2$, the energy of formation of which (193.63 kcal/mol) is lower than the energy of formation of the vertically ionized structure by only 1.26 kcal/mol. However, the symmetry decrease from C_{2v} to C_s, which results in the radical

Table 1. Geometry parameters (bond lengths, Å; angles, deg) of the molecule (RHF) and five electronic states of the radical cation (UHF) of 1,3-DMA* calculated by the PM3 method

Bond, angle	Molecule	Radical cation				
	C_{2v}	C_{2v}, $8B_1$	C_s, $20A'$	C_{2v}, $9B_2$	C_s, $15A'$	C_{2v}, $12A_1$
C_1–C_2	1.5295	1.5604	1.5613	1.5275	1.5278	1.5246
C_2–C_3			1.5166		1.5287	
C_1–C_4	1.5290	1.5043	1.5191	1.5320	1.5393	1.5265
C_1–C_6					1.5191	
C_3–C_5			1.4997		1.5393	
C_3–C_7					1.5191	
C_4–C_8	1.5370	1.5557	1.5283	1.5127	1.4913	1.5427
C_6–C_9					1.5380	
C_5–C_8			1.6082		1.4913	
C_7–C_9					1.5380	
C_8–C_{10}	1.5366	1.5267	1.5207	1.6193	2.0252	1.5363
C_9–C_{10}					1.5040	
C_8–C_{11}	1.5233	1.5177	1.5178	1.5312	1.4827	1.5308
C_9–C_{12}					1.5350	
C_1–H	1.1152	1.1357	1.1182	1.1156	1.1168	1.1249
C_3–H			1.1543		1.1167	
C_2–H_a	1.1072	1.1061	1.1074	1.1081	1.1079	1.1090
C_2–H_b					1.1079	
C_4–H_a	1.1077	1.1112	1.1116	1.1099	1.1117	1.1111
C_5–H_a			1.1074			
C_6–H_a			1.1116		1.1094	
C_7–H_a			1.1074			
C_4–H_b	1.1077	1.1089	1.1101	1.1115	1.1158	1.1096
C_5–H_b			1.1074			
C_6–H_b			1.1101		1.1091	
C_7–H_b			1.1074			
C_{10}–H_a	1.1083	1.1112	1.1148	1.1045	1.0947	1.1093
C_{10}–H_b			1.1119			
C_{11}–H_a	1.0981	1.0987	1.0989	1.1029	1.1044	1.0984
C_{12}–H_a					1.0989	
C_{11}–H_b	1.0981	1.0989	1.0991	1.0988	1.1005	1.0984
C_{12}–H_b					1.0982	
C_{11}–H_c			1.0991		1.1005	
C_{12}–H_c					1.0982	
C_1–C_2–C_3	109.4	101.3	105.1	109.9	109.4	110.2
C_4–C_1–C_6	109.6	112.6	111.4	107.3	110.0	112.0
C_5–C_3–C_7			113.4			
C_8–C_{10}–C_9	110.4	111.5	112.1	102.9	104.9	112.0
C_{10}–C_8–C_{11}	110.0	111.1	112.0	99.2	101.8	113.0
C_{10}–C_9–C_{12}					105.2	
H–C_1–C_2	109.5	99.7	106.9	110.0	109.6	112.0
H–C_3–C_2			105.9			
H_a–C_2–H_b	106.2	108.0	106.9	105.7	105.6	106.5
H_a–C_{10}–H_b	106.1	104.7	104.3	109.2	119.9	107.4

* See Fig. 4 for the numbering of atoms and the shapes of the HOMO of the molecule and the SOMO of the 1,3-DMA radical cation.

Table 2. Isotropic hyperfine-interaction constants with hydrogen atoms (a_{iso}^{H}, G) for five electronic states of the 1,3-DMA* radical cation calculated by the PM3-UHF method

Bond	Radical cation				
	C_{2v}, $8B_1$	C_s, $20A'$	C_{2v}, $9B_2$	C_s, $15A'$	C_{2v}, $12A_1$
C_1–H	99.4	14.3	–1.3	0.3	42.4
C_3–H		168.3			
C_2–$H_{a, b}$	–6.3	–1.3	3.5	0.2	9.5
C_4–H_a	26.3	29.6	1.8	9.4	15.0
C_5–H_a		–0.4			
C_6–H_a		29.6		–0.3	
C_7–H_a		–0.4			
C_4–H_b	–0.8	3.8	28.0	41.8	8.3
C_5–H_b		–0.7			
C_6–H_b		3.8		–0.6	
C_7–H_b		–0.7			
C_{10}–H_a	16.2	46.5	–10.2	–9.9	12.6
C_{10}–H_b		9.7			
C_{11}–H_a	0.4	0.1	34.3	29.3	–0.8
C_{12}–H_a				3.0	
C_{11}–H_b	3.6	0.9	–2.2	5.0	2.3
C_{12}–H_b				–1.6	
C_{11}–H_c		9.9		5.0	
C_{12}–H_c				–1.6	
⟨S**2⟩	0.7579	0.7587	0.7573	0.7594	0.7542

* See Fig. 4 for the numbering of atoms and the shapes of the HOMO of the molecule and the SOMO of the 1,3-DMA radical cation; the calculation procedure for the isotropic hyperfine-interaction constants a_{iso}^{H} is specified in Experimental.

cation structure of interest with SOMO of symmetry $15A'$, is accompanied by a dramatic (by 10.11 kcal/mol) stabilization of the structure, the energy of formation of which (183.52 kcal/mol) is the lowest of those calculated by the PM3 method. The structure of the 1,3-DMA radical cation with SOMO of symmetry $12A_1$ (C_{2v}), which was excluded from consideration, is characterized by the greatest energy of formation (195.59 kcal/mol). This adiabatic ionization energy is higher than the (initial) vertical ionization energy of 1,3-DMA by 0.7 kcal/mol.

Table 1 summarizes the geometry parameters of the molecule and the four 1,3-DMA radical cation species under discussion. A comparison between data on the two radical cations of symmetry C_s indicates that the radical cation with SOMO of symmetry $15A'$ really corresponds to the ionization of a single C_8–C_{10} bond, which is elongated to a "critical" value of about 2 Å (2.0252 Å). This considerable elongation of a chosen C–C bond in the radical cations of hydrocarbons is somewhat overestimated by the PM3 method; however, it is typical (1.8–2.0 Å) and consistent with the results of more precise ab initio and DFT calculations [12, 20, 22]. In the case of the 1,3-DMA radical cation, this structure is stabilized as a result of the partial separation of positive-charge and spin-density distributions. The charge is primarily localized at the tertiary C_8 atom, whereas the spin density is localized at the C_{10} atom. In the radical cation with SOMO of symmetry $20A'$, two C–C bonds (C_5–C_8 and C_7–C_9), as well as the C_3–H bond, which is elongated to 1.1543 Å, undergo the greatest elongation (to 1.6082 Å).

A correspondence between the calculated and experimental constants a_{iso}^{H} is of crucial importance for the assignment of a particular calculated radical cation structure to the measured EPR spectrum. Table 2 summarizes the constants a_{iso}^{H} calculated by the PM3 method for all of the five forms of the 1,3-DMA radical cation. It can be seen in Table 2 that the set of experimental constants a_{iso}^{H} = 145 (1 H), 40 (1 H), and 20 G

(2 H) corresponds to the only C_s-symmetric radical cation structure with SOMO of symmetry 20*A*', which is characterized by the set of calculated constants a_{iso}^{H} = 168.3 (1 H), 46.5 (1 H), and 29.6 G (2 H), which is consistent with the experimental set. Only a small systematic overestimation of the values of a_{iso}^{H} was observed. Thus, the results of the PM3 quantum-chemical analysis lend support to the validity and unambiguity of the previous tentative assignment of the EPR spectrum to the 1,3-DMA radical cation structure with a chosen tertiary C–H bond (see Fig. 3). All of the calculated forms of the 1,3-DMA radical cation are characterized by reasonable values of $\langle s^{**}2\rangle$ (see Table 2), which are close to the theoretical value $\langle s^{**}2\rangle = 0.75$ for spin $s = 1/2$.

Figure 5 shows selected geometry parameters (calculated by the PM3 method) of the molecules and radical cations of related structures: (a) adamantane, (b) 1,3-DMA, and (c) 1,*cis*-3,*trans*-5-trimethylcyclohexane (TMCH). Figure 5 also shows the constants a_{iso}^{H} obtained by the specified method, as compared with the experimental values. The geometric structure of the adamantane radical cation was determined previously by DFT and ab initio methods without the use of EPR data, which are unavailable [12, 27–30]. In contrast, only EPR data are available for the TMCH radical cation; the accuracy of these data was supported by only trial calculations with the use of MNDO and INDO semiempirical methods [31]. Therefore, we calculated energy and geometry characteristics and the constants a_{iso}^{H} for all of the three related structures using the same PM3 method.

As can be seen in Fig. 5, the three parent molecules have practically equal lengths of C–C bonds in the cyclohexane fragment and tertiary C–H bonds. The adiabatic ionization potentials PI_a, the structures of radical cations, and the elongations $\Delta CH = CH_{RC} - CH_{mol} \sim 0.04$ Å are also close to each other and consistent with available published data [12, 27–31]. As compared with the adamantane radical cation, in which three C–C bonds are equally elongated (to 1.585 Å), two C–C bonds in the 1,3-DMA radical cation are even more elongated (to 1.608 Å) and the third bond is noticeably shortened (to 1.561 Å). Thus, the structure of the 1,3-DMA radical cation is somewhat closer to the structure of the TMCH radical cation, in which two analogous C–C bonds are approximately equally elongated (to 1.593 Å), rather than to the geometric structure of the adamantane radical cation. However, an analysis of the SOMO composition and the constants a_{iso}^{H} indicates that all of the three radical cations not only exhibit qualitatively identical electronic structures of the cyclohexane–adamantane fragment with a chosen tertiary C–H bond but also are characterized by almost equal calculated values of the greatest (~170 G (1 H)) and the second greatest constant a_{iso}^{H} (40–60 G (1 H)).

Thus, the data on the structure of the 1,3-DMA radical cation are consistent with the available data on the structures of the adamantane and TMCH radical cations, as well as with the reactivity of the 1,3-DMA radical cation under model radiation-chemical conditions, that is, with the selective deprotonation of a weakened tertiary C–H bond, which results in a neutral tertiary radical of the adamantyl type (see Fig. 3). Consequently, it is reasonable to hypothesize that the new biomimetic mechanism of the selective formation of a tertiary alcohol from 1,3-DMA in the test catalytic Gif-type system is related to the intermediate formation of the 1,3-DMA radical cation (SOMO of symmetry $8B_1$) and the high selectivity of its subsequent transformations, which occur with the participation of a weakened tertiary C–H bond.

DISCUSSION

1. Selectivity of the Oxidation and Oxidative Functionalization of Cage Saturated Hydrocarbons from the Standpoint of the Deprotonation Selectivity of Their Radical Cations

The empirical rule according to which the radical cations of organic substrates undergo selective deprotonation refers to model radiation-chemical conditions. The reason for this behavior of radical cations is that, of many activated C–H bonds in the radical cations, only the C–H bond that is activated to the greatest extent is involved in chemical transformations. In other words, of many possibilities, only one reaction path occurs in the case of radical cations; this reaction path depends on the SOMO of the radical cation and a particular chemical environment.

We believe that this selectivity of processes with the participation of radical cations is a universal property. Radical cations exhibit this property not only under model radiation-chemical conditions but also under any conditions including the conditions of a real chemical experiment. The occurrence of several reaction products in the one-electron oxidation of substrate molecules may only mean that the radical cations under reaction conditions occur in various particular environments, which can change the kind of SOMO (for several substrates) and, consequently, affect the selectivity of processes with the participation of radical cations. It is likely that, more commonly, the kind of SOMO is retained with changes in the particular environment but the partner of the radical cation in the ion–molecule reaction changes to result in various versions of this reaction.

This methodology was accepted for the analysis of the chemical behavior of the 1,3-DMA radical cation under the test catalytic conditions. The most activated tertiary C–H bond of the 1,3-DMA radical cation was capable of either undergoing deprotonation or adding

the acetonitrile molecule or the oxygen atom of a ferroxo complex [9].

The first formulated general method for the selectivity analysis of reactions involving radical cations under various conditions allowed us to compare data of radiation-chemical and chemical experiments and to predict the possible participation of radical cations in various chemical processes, in which the direct detection of short-lived radical cations is difficult to perform.

In this section, we give an additional illustration to the universal selectivity rule, as applied to the analysis of deprotonation directions in the radical cations of cage saturated hydrocarbons, which simultaneously contain tertiary and secondary C–H bonds, in order to demonstrate that both tertiary and secondary C–H bonds can be activated depending on the kind of the SOMO of the radical cation. In these cases, a clear correspondence between the direction of the selective deprotonation of radical cations under model radiation-chemical conditions and the composition of oxidation and oxidative functionalization products of the same cage saturated hydrocarbons under conditions of a real chemical experiment is observed. This correspondence takes place under the action of reagents that can serve as one-electron oxidants.

As an example, the following four hydrocarbons were chosen: 1,3-DMA, adamantane (Fig. 6), bicyclo[2.2.1]heptane (norbornane), and bicyclo[2.2.2]octane (Fig. 7). Upon the ionization of 1,3-DMA and adamantane, tertiary C–H bonds are activated. Under model radiation-chemical conditions, the secondary radicals of 1,3-DMA were not observed. Analogously, this process should not be expected in the case of adamantane, for which only data on the products of chemical and electrochemical oxidation [10–16] and the results of quantum-chemical calculations [12, 27–30] are available. In the cases when 1,3-DMA and adamantane were subjected to one-electron oxidation under identical conditions, they exhibited the same reactivity [11].

According to data obtained by photoelectron spectroscopy, the first vertical ionization potentials PI_v (eV) of adamantane, a number of its methyl-substituted derivatives, and oxidation products (tertiary and secondary alcohols and a ketone) have practically equal values of 9.20–9.28 eV [14, 31–34]. It is likely that the value PI_v = 8.76 eV for adamantanone is somewhat underestimated because PI_v = 9.06 eV for 2,6-adamantanedione [34]. The constancy of PI_v for the above compounds from the adamantane series suggests that the uniform ionization of the adamantane skeleton with the activation of tertiary C–H bonds occurs in all cases.

The main product of the oxidation of adamantane with the use of CrO_3 in $AcOH/Ac_2O$, as well as of 1,3-DMA with the use of Fe^{2+}/H_2O_2 (experiment no. 13 [9]), is a tertiary alcohol (71%) [35]. Adamantanone (6%) is a by-product, whose concentration is consistent with a small amount (4%) of 1,3-DMA oxidation products at secondary C–H bonds in experiment no. 13. The ability of Cr^{6+} compounds to oxidize adamantane hydrocarbons by a one-electron mechanism was demonstrated using quantum-chemical calculations [12].

Bicyclo[2.2.1]heptane and bicyclo[2.2.2]octane exhibit somewhat higher ionization potentials (PI_v = 9.80 and 9.53 eV, respectively [32, 34]) than adamantane and its derivatives. Under model radiation-chemical conditions, the shape of SOMO in the radical cations of these two cage saturated hydrocarbons and the radical cation deprotonation products (free radicals) were determined [18]. In accordance with the shape of SOMO, by the empirical rule cited in the Introduction, secondary rather than tertiary C–H bonds undergo selective activation followed by deprotonation. In accordance with this, under the same oxidation conditions (CrO_3 in $AcOH/Ac_2O$), both of the above hydrocarbons are selectively oxidized to ketones (main products) and 2-aceto derivatives (Fig. 7) [35]. In the case of both of the bicyclic compounds, products of oxidation at tertiary C–H bonds (a tertiary alcohol and 1-aceto derivatives) were not observed.

Thus, under the same conditions (CrO_3 in $AcOH/Ac_2O$), both tertiary and secondary C–H bonds in cage saturated hydrocarbons can be selectively activated in accordance with the shape of the SOMO of the radical cation and, probably, with the shape of the HOMO of the parent molecule. This approach to an analysis of the reactivity of saturated hydrocarbons under various oxidation conditions has a predictive capacity and can serve as an additional tool in studying the mechanisms of reactions in which the intermediate formation of radical cations may be assumed.

2. Concerted Mechanism of the Insertion of the Oxygen Atom of the Ferroxo Complex $Fe^{n+2}=O$ (n = 2, 3) into an Activated Tertiary C–H Bond of the 1,3-DMA Radical Cation under New Standard Conditions (Experiment No. 13 [9])

A stable product with the molecular ion $M^{+\cdot}$ 205 was a by-product in the oxidation of 1,3-DMA under initial standard conditions (experiment no. 1) [9]. We believe that the nitrogen atom in this azomethine (Schiff base) is attached to the adamantane fragment at the tertiary position, that is, in the same manner as pyridine fragments are attached [9]. The formation of this compound was not detected previously.

A two-electron mechanism usually occurred in the electrochemical and chemical oxidation of adamantane and its 1-substituted alkyl derivatives. According to this mechanism, 1-adamantylacetamide and 1-alkyl-3-acetamide derivatives of adamantane were final products after hydrolysis (Fig. 8a) [10, 11, 13–16, 33]. This two-electron oxidation of adamantane and its 1-aklyl derivatives occurred because the first vertical ionization

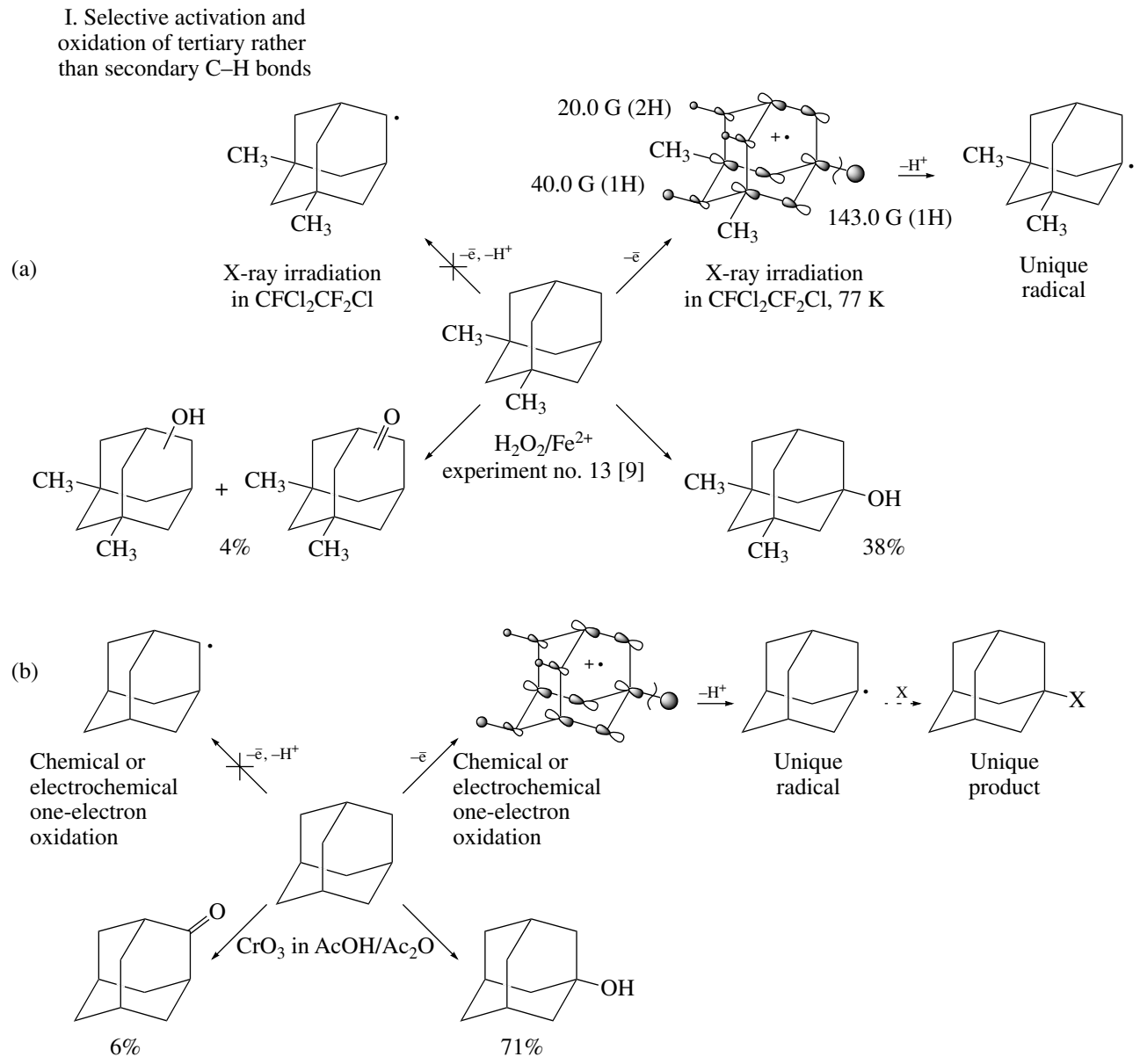

Fig. 6. Correspondence between the selective activation of tertiary rather than secondary C–H bonds in the radical cations of cage saturated hydrocarbons and the selective oxidation of tertiary rather than secondary C–H bonds in the above hydrocarbons, as exemplified by (a) 1,3-DMA and (b) adamantane.

potential PI_v of neutral radicals is much lower than that of parent hydrocarbons. Thus, PI_v = 9.20–9.28 eV for adamantane and 6.30 or 6.85 eV for 1-adamantyl or 2-adamantyl radicals, respectively [36].

The results of quantum-chemical calculations performed by DFT methods [12, 27] are the only example that clarifies the possible formation of an azomethine (Schiff base) (Fig. 8b). The compound of interest can result from the one-electron mechanism of the concerted insertion of the nitrogen atom of the acetonitrile molecule into the activated tertiary C–H bond of the radical cations of adamantane and its 1-alkyl derivatives. According to calculations, the acetonitrile molecule can significantly stabilize (by 12.8 kcal/mol) the radical cation structure of adamantane. The radical cation structure formed as a result of the insertion of the nitrogen atom of the acetonitrile molecule into the activated tertiary C–H bond of the adamantane radical cation (stabilization by 9.5 kcal/mol) is energetically favorable. With reference to the adamantane radical cation, the intermediate insertion structure requires the consumption of 7.2 kcal/mol. Path (a) of the further stabilization of the addition product by the migration of a hydrogen atom from the nitrogen atom to the carbon atom followed by the reduction of electric neutrality of the final compound might lead to the structure of inter-

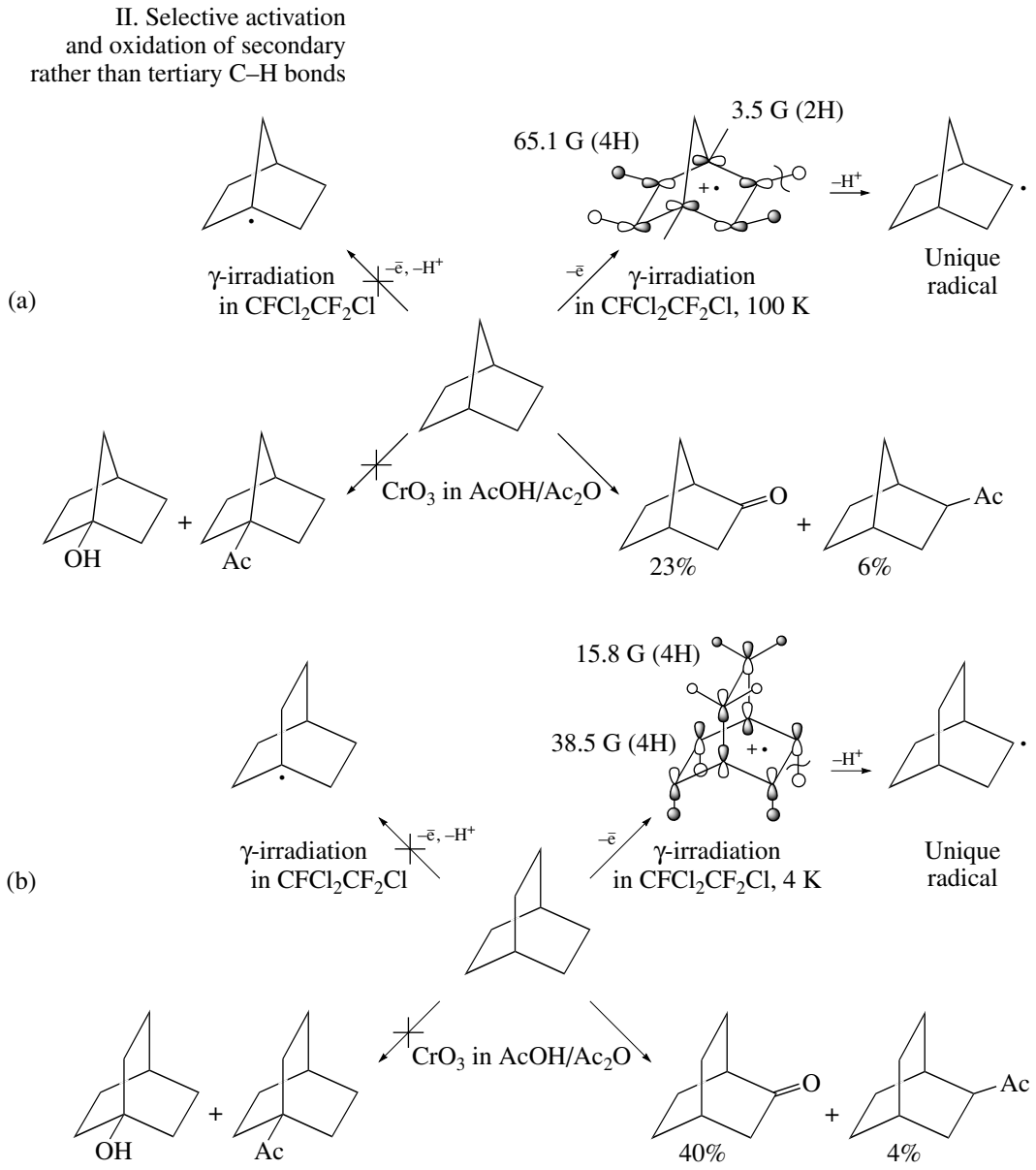

Fig. 7. Correspondence between the selective activation of secondary rather than tertiary C–H bonds in the radical cations of cage saturated hydrocarbons and the selective oxidation of secondary rather than tertiary C–H bonds in the above hydrocarbons, as exemplified by (a) bicyclo[2.2.1]heptane and (b) bicyclo[2.2.2]octane.

est. The abstraction of this hydrogen atom could result in the nitrile cation structure (path (b)). In our experiments, we tested the presence of the 1-acetamide derivative of 1,3-DMA. It was detected only in trace amounts.

The main special feature of 1,3-DMA oxidation with the use of hydrogen peroxide under new standard conditions (experiment no. 13 [9]) consists in the complete absence of products of pyridine and acetonitrile alkylation by the adamantane framework of 1,3-DMA. This fact suggests that, under the new conditions used, the deprotonation of the 1,3-DMA radical cation did not occur with the formation of a tertiary free radical, which could escape into the reaction volume (Fig. 1, path 2a; see also Fig. 6 in [9]). Moreover, the absence of an azomethine (product with $M^{+\cdot}$ 205) may indicate that the 1,3-DMA radical cation also had no time to escape to the reaction volume of the solvent (Fig. 1, path 2b; see also Fig. 5 in [9]). These observations allowed us to assume that, under the new standard conditions (experiment no. 13 [9]), a more rapid process occurred: the concerted insertion of the oxygen atom of the oxidizing catalytic center into the activated tertiary C–H bond of the 1,3-DMA radical cation (Fig. 1, path 2c; see also Fig. 5 in [9]). To the best of our knowledge, this possibility was not discussed previously.

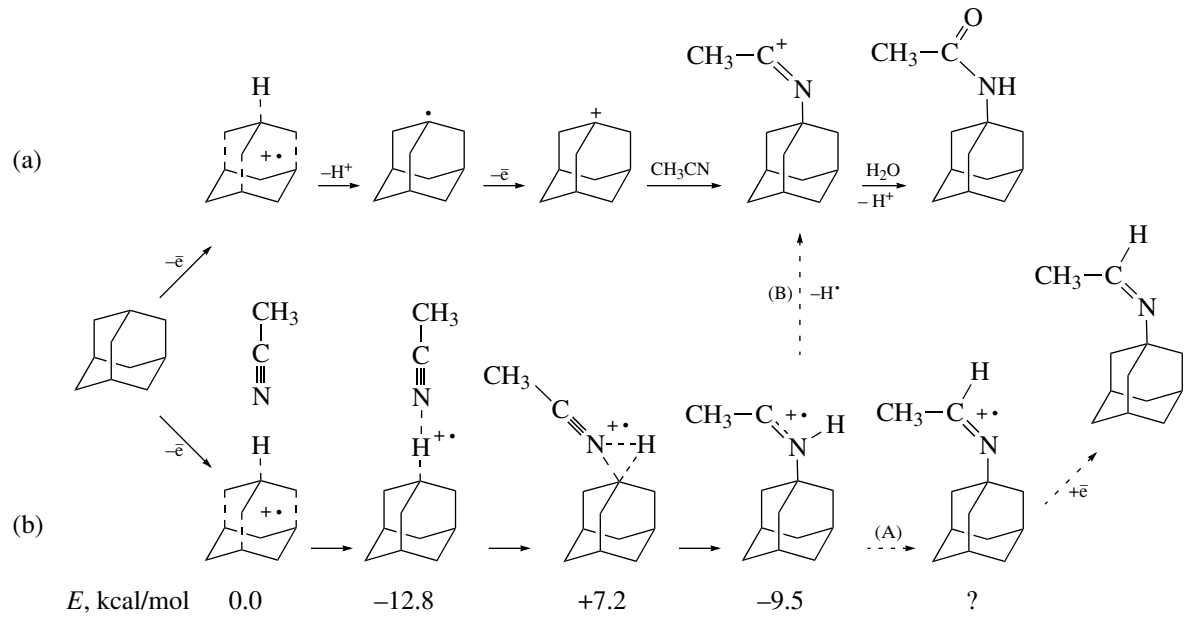

Fig. 8. Mechanisms and products of (a) two-electron and (b) one-electron oxidation of adamantane in acetonitrile. Dashed lines show our supplements to possible paths (A) and (B). See the test for details.

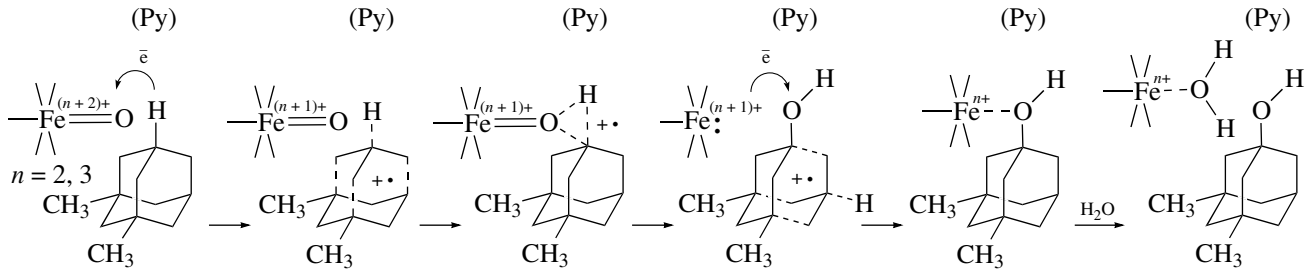

Fig. 9. Hypothetical mechanism of the formation of the 1,3-DMA radical cation and the concerted insertion of the oxygen atom of a ferroxo complex into the activated C–H bond of the 1,3-DMA radical cation in an explicit form.

Figure 9 shows a detailed reaction scheme (separated into steps for convenience) for the proposed concerted mechanism of the insertion of the oxygen atom of the ferroxo complex Fe^{n+2}=O (where n = 2, 3) into the tertiary C–H bond of 1,3-DMA activated by the one-electron oxidation of the substrate (first step). As a result of this, the 1,3-DMA radical cation is formed as an intermediate. At the second step, a three-center complex is formed with the participation of the oxygen atom and the carbon and hydrogen atoms of the activated tertiary C–H bond of the 1,3-DMA radical cation. The stabilization of this transition complex can facilitate the coordination of the nitrogen atom of the pyridine molecule to oxygen or hydrogen atoms. As a result of this stabilization, that is, a decrease in the energy of formation, the rate of the subsequent insertion of the oxygen atom (oxene) into the activated C–H bond of the hydrocarbon radical cation can increase. Because of this, reaction paths 2a and 2b in Fig. 1 can have no time to occur. Recall that pyridine is a necessary component of the catalytic system [9]. At the third step, the oxygen atom is inserted into the activated tertiary C–H bond of the 1,3-DMA radical cation. As a result, the radical cation of a tertiary alcohol of 1,3-DMA is formed. As noted above, the replacement of a hydrogen atom by a hydroxyl group does not change the vertical ionization potential of the adamantane skeleton (PI_v = 9.20–9.28 eV). By this is meant that the SOMO of the radical cation does not enclose the more electronegative oxygen atom, which increases the ionization potential, that is, the C–O and C–H bonds. In Fig. 9, this situation is reproduced by a change in the orientation of the SOMO of the radical cation, which is concentrated on the adamantane fragment. The remaining tertiary C–H bond is activated under changes in the SOMO orientation. At the fourth step, the electrically neutral structure of the tertiary alcohol, which remains in the coordination sphere of the iron ion Fe^{n+}, is restored. At the final fifth step, the water molecule substitutes for the tertiary

alcohol in the coordination sphere of the iron ion Fe^{n+} to release the tertiary alcohol into the bulk solvent.

The question of whether the final fifth step occurs during catalytic oxidation or only at the instant the reaction mixture is decomposed with water after completion of the experiment is still an open question.

The questions of which of the iron species Fe^{2+} or Fe^{3+} forms the catalytic center and what is its real structure remain unanswered. Therefore, in the reaction sequence shown in Fig. 9, the catalytic center is given in the generalized form Fe^{n+2+}=O (where n = 2, 3) without the specification of a ligand environment. It is well known that both of the ferroxo complexes Fe^{5+}=O and Fe^{4+}=O can selectively oxidize saturated hydrocarbons to alcohols [3].

The concerted mechanism (Fig. 1, path 2c; detailed reaction scheme in Fig. 9; see also Fig. 6 in [9]) proposed for the oxidation of 1,3-DMA to a tertiary alcohol with the intermediate formation of the 1,3-DMA radical cation is largely analogous to the one-electron mechanism of acetonitrile alkylation by adamantane (at nitrogen), which was proposed by Fokin with coauthors [12, 27] and shown in Fig. 8b.

ACKNOWLEDGMENTS

We are grateful to R.M. Varushchenko for providing us with a high-purity 1,3-DMA sample (99.93%) [37].

REFERENCES

1. *Activation and Functionalization of Alkanes*, Hill, C., Ed., New York: Wiley, 1989.
2. *Electron Transfer in Chemistry*, Balzani, V., Ed., New York: Wiley-VCH, 2001.
3. Shilov, A.E. and Shul'pin, G.B., *Aktivatsiya i kataliticheskie reaktsii uglevodorodov* (Activation and Catalytic Reactions of Hydrocarbons), Moscow: Nauka, 1995, p. 399.
4. Slepen'kin, A.V., Akkerman, S.B., Dolgopolova, T.N., et al., *Neftekhimiya*, 1993, vol. 33, no. 5, p. 406.
5. Barton, D.H.R., Gastiger, M.J., and Motherwell, W.B., *J. Chem. Soc., Chem. Commun.*, 1983, no. 1, p. 41.
6. Barton, D.H.R., *Tetrahedron*, 1998, vol. 54, p. 5805.
7. Kiani, S., Tapper, A., Staples, R.J., and Stavropoulos, P., *J. Am. Chem. Soc.,* 2000, vol. 122, no. 31, p. 7503.
8. Stavropoulos, P., Celenligil-Cetin, R., and Tapper, A.E., *Acc. Chem. Res.*, 2001, vol. 34, no. 9, p. 745.
9. Vasil'eva, V.V., Nekhaev, A.I., Shchapin, I.Yu., and Bagrii, E.I., *Kinet. Katal.*, 2006, vol. 47, no. 4, p. 610 [*Kinet. Catal.* (Engl. Transl.), vol. 47, no. 4, p. 627].
10. Mella, M., Freccero, M., Soldi, T., et al., *J. Org. Chem.*, 1996, vol. 61, no. 4, p. 1413.
11. Ishii, Y., Matsunaka, K., and Sakaguchi, S., *J. Am. Chem. Soc.*, 2000, vol. 122, no. 30, p. 7390.
12. Fokin, A.A. and Schreiner, P.R., *Chem. Rev.,* 2002, vol. 102, no. 5, p. 1551.
13. Jones, S.R. and Mellor, J.M., *J. Chem. Soc., Chem. Commun.*, 1976, no. 11, p. 385.
14. Edwards, G.J., Jones, S.R., and Mellor, J.M., *J. Chem. Soc., Perkin Trans. 2,* 1977, no. 4, p. 505.
15. Yoshida, K., *Electrooxidation in Organic Chemistry: The Role of Cation Radicals As Synthetic Intermediates*, New York: Wiley, 1984.
16. *Organic Electrochemistry: An Introduction and a Guide*, Baizer, M.M. and Lund, H., Eds., New York: Marcel Dekker, 1983.
17. *Topics in Molecular Organization and Engineering,* Lund, A. and Shiotani, M., Eds., Dordrecht: Kluwer, 1991, vol. 6, p. 496.
18. Numome, K., Toriyama, K., and Iwasaki, M., *Tetrahedron,* 1986, vol. 42, no. 22, p. 6315.
19. Shchapin, I.Yu., Fel'dman, V.I., Belevskii, V.N., et al., *Izv. Akad. Nauk, Ser. Khim.*, 1995, no. 2, p. 212.
20. Shchapin, I.Yu. and Chuvylkin, N.D., *Izv. Akad. Nauk, Ser. Khim.*, 1996, no. 2, p. 321.
21. Shchapin, I.Yu., Belopushkin, S.I., Tyurin, D.A., et al., *Dokl. Akad. Nauk*, 2000, vol. 372, no. 1, p. 60 [*Dokl. Chem.* (Engl. Transl.), vol. 372, nos. 1–3, p. 81].
22. Shchapin, I.Yu., Belopushkin, S.I., Tyurin, D.A., et al., *Rus. J. Phys. Chem.*, 2000, vol. 74, Suppl. 2, p. S292.
23. Stewart, J.J.P., *MOPAC 7.00, Public Domain Copy,* Frank J. Seiler Research Laboratory, US Air Force Academy, Colorado Springs, USA, 1993.
24. Chuvylkin, N.D. and Tomachev, A.M., *Izv. Akad. Nauk, Ser. Khim.*, 1999, no. 2, p. 245.
25. Krusic, P.J., Petty, T.A., and Schleyer, P.R., *J. Am. Chem. Soc.*, 1972, vol. 94, no. 3, p. 995.
26. Vikulin, V.V., Klinshpont, E.R., and Podkhalyuzin, A.T., *Khim. Vys. Energ.*, 1978, vol. 12, no. 2, p. 85.
27. Fokin, A.A., Schreiner, P.R., Gunchenko, P.A., et al., *J. Am. Chem. Soc.,* 2000, vol. 122, no. 30, p. 7317.
28. Fokin, A.A., Shubina, T.E., Gunchenko, P.A., et al., *J. Am. Chem. Soc.,* 2002, vol. 124, no. 36, p. 10718.
29. Fokin, A.A., Gunchenko, P.A., Peleshanko, S.A., et al., *Eur. J. Org. Chem.,* 1999, no. 4, p. 855.
30. Shubina, T.E., Gunchenko, P.A., Yurchenko, A.G., et al., *Teor. Eksp. Khim.*, 2002, vol. 38, no. 1, p. 8.
31. Shiotani, M., Lindgren, M., and Ichikawa, T., *J. Am. Chem. Soc.*, 1990, vol. 112, no. 3, p. 967.
32. Bodor, N., Dewar, M.J.S., and Worley, S.D., *J. Am. Chem. Soc.*, 1970, vol. 92, no. 1, p. 19.
33. Miller, L.L., Koch, V.R., Koenig, T., and Tuttle, M., *Tetrahedron Lett.*, 1973, vol. 95, no. 15, p. 5075.
34. Gurvich, L.V., Karachintsev, G.B., and Kondrat'ev, V.N., *Energii razryva khimicheskikh svyazei. Potentsialy ionizatsii i srodstvo k elektronu* (Bond Dissociation Energies, Ionization Potentials, and Electron Affinity), Moscow: Nauka, 1974.
35. Bingham, R.C. and Schleyer, P.V.R, *J. Org. Chem.*, 1971, vol. 36, no. 9, p. 1198.
36. Mel'nikov, M.Ya. and Smirnov, V.A., *Fotokhimiya organicheskikh radikalov* (Photochemistry of Organic Radicals), Moscow: Mosk. Gos. Univ., 1994.
37. Varushchenko, R.M., Druzhinina, A.I., Senyavin, V.M., and Sarkisova, V.S., *J. Chem. Thermodyn.*, 2004, vol. 33, no. 2, p. 141.